mathematics

MDPI

Article

An Adaptive Frequency Sampling Algorithm for Dynamic Condensation-Based Frequency Response Analysis

Jaehun Lee [1,*], Younggeun Park [1], Yeji Lee [1] and Seongmin Chang [2,*]

[1] Department of Mechanical, Robotics and Energy Engineering, Dongguk University, Seoul 04620, Republic of Korea
[2] School of Mechanical Engineering, Chungnam National University, Daejeon 34134, Republic of Korea
* Correspondence: jaehun@dgu.edu (J.L.); schang@cnu.ac.kr (S.C.); Tel.: +82-2-2260-3826 (J.L.)

Abstract: This paper proposed an efficient and adaptive frequency sampling algorithm for frequency response analysis using dynamic condensation-based reduced-order modeling. For the degree of freedom-based model reduction method, the reduced-order basis becomes a frequency-dependent matrix since the relationship between master and slave degrees of freedom stems from partial equations of a second-order dynamical system. Such frequency-dependency makes the analysis inefficient for investigating the frequency response of the system. Considering that the coverage of a local reduced-order basis at a single frequency varies depending on the frequency, a new frequency sampling algorithm was proposed with a strategy of constructing multiple local reduced-order models (ROMs) at sample frequencies. For adaptive sampling, the frequency range of a local ROM was evaluated, and a new sample was added if there was a gap between two adjacent ROMs. As a result, the accuracy of the local ROM can be estimated, and the efficiency in the online stage was greatly enhanced. The proposed method was verified by performing frequency response analysis with several numerical examples, including a large-scale structural and dynamic system.

Keywords: reduced-order modeling; dynamic condensation; frequency response analysis; adaptive frequency sampling

MSC: 70-08

Citation: Lee, J.; Park, Y.; Lee, Y.; Chang, S. An Adaptive Frequency Sampling Algorithm for Dynamic Condensation-Based Frequency Response Analysis. *Mathematics* **2023**, *11*, 2683. https://doi.org/10.3390/math11122683

Academic Editor: Gaohui Wang

Received: 8 May 2023
Revised: 2 June 2023
Accepted: 12 June 2023
Published: 13 June 2023

1. Introduction

As the requirement for complex and sophisticated modeling of structural systems has increased continuously, demands efficient surrogate models have also increased since they can provide accurate and reliable solutions to various problems of interest in a timely fashion. Particularly, reduced-order models (ROM) derived from the original full-order model (FOM) guarantee more robust input-output relations than pure data-fit approaches [1,2]. Therefore, ROMs are frequently used when we face time-critical applications that also require a certain level of accuracy.

Most of the model order reduction techniques rely on the projection of the FOM to a subspace containing the physical properties of a given system. For linear, time-invariant dynamical systems, eigenmodes from mass and stiffness matrices can be a projector that transforms FOM to a generalized coordinate system of a subspace. In this case, a linear combination of the portion of the column-wise projection matrix and the unknown variable can describe the approximated behavior of the system. Thus, the main characteristic of the ROM is determined by that of the reduced-order basis (ROB, i.e., projection matrix). Several approaches have been popularly used for analyzing complicated dynamical systems [3–5]. Recently, the ROMs for dynamic systems are extending their scalabilities by combining with data-driven approaches in a non-intrusive manner showing efficient approximations for the behavior of complex systems [6,7], retaining selected physical information [8], computing

structural responses including sensitivities [9], and can be extended to various engineering disciplines including acoustic-structural multiphysics problems [10].

One fundamental property to be addressed in this research is that most ROBs transform FOM into generalized coordinate systems. As a result, a recovery process is mandatory for the approximation of the FOM. If the ROB is derived considering the relationship between each degree of freedom in physical coordinates, the reduced variable can present the same property in the physical domain. We refer to such methods as the degree of freedom-based reduced-order model [11,12], also known as a static (or dynamic) condensation [13,14]. Research on DOF-based ROM is relatively less active than those on mode-based ROM due to the convenience of constructing ROBs in generalized coordinates. However, because the physical DOF of the ROM can be synchronized with the actual sensor location directly, DOF-based ROM can be a powerful tool, particularly when we consider data acquisition-based modeling and simulations [15], system identification based on sensor data [16], model updating techniques and experiments [17], and so on. Meanwhile, for transformation between reduced variables in modal coordinates and those in physical coordinates, the SEREP method [18] can be applied by dividing ROM into parts of master and slave DOF with pseudo-inverse of the partitioned ROB. Thus, one can acquire the advantage of DOF-based ROM even when using ROB of generalized coordinates.

Another motivation of the present research is that most ROBs are not adaptive to parameters of interest such as the frequency in this research. Usually, various physical properties such as geometric and material properties, initial and boundary conditions, loading conditions, and uncertainties are system parameters. Thus, to efficiently approximate output quantities of interest into input parameter change, various research has been performed within the parametric reduced-order model (PROM) framework. There are several approaches for considering parametric variations, including using global ROBs [19–21], manifold interpolation-based approaches [22–24], perturbation-based methods [25,26], introducing domain decomposition methods [27–29] or Sherman-Morrison-Woodbury formula [30], using conventional interpolations, or enhanced interpolation scheme [31,32] and so on. The basic procedure of the PROM is decomposing the system or the ROB into parameter-dependent and -independent terms. Parameter-dependent terms can be either a basis of a function space or a weighting function. Parameter-independent terms are data acquired from multiple offline simulations or parts derived by extracting parameter-dependent terms from original matrices during the modeling procedure. By a linear combination of the two terms, ROB can be adapted to the new input value of the parameter.

On the other hand, the Krylov subspace method and Padé approximation method [33–37] have been used in a similar context with PROM, one of the most popular methods for frequency sweep analysis. The methods approximate frequency responses by deriving the coefficient of the interpolation function from the differentiation of the governing equation at the upper and lower bounds of the frequency range of interest. Results show that interpolatory ROM is efficient with an ability to adaptively control accuracy by adding more sample points.

In the present work, localization of the ROB with an adaptive frequency sampling strategy was proposed within the framework of dynamic condensation. Specifically, multiple transformations and associated ROMs were constructed from several sampling frequency instances. Sampling ranges were adaptively refined considering the difference between two adjacent ROMs. Previously, dynamic condensation considering the dependency of the ROB on the frequency and its variants has been introduced in the literature [13,15]. However, performing an inversion of a dynamic stiffness matrix corresponding to parts of the slave DOF at every frequency is neither efficient nor appropriate. In general, the number of master DOFs is much less than that of slave DOFs since there are limited sensors in a real situation. Thus, the inverse of the dynamic stiffness of the slave DOF is not as efficient as that of a full system matrix. This computational burden can be relieved by constructing multiple ROMs at sample frequencies and using them depending on a new input frequency. For such an offline-online procedure, the offline phase should not be overridden, as multiple high-fidelity simulations require significant computational resources. Thus,

an efficient sampling strategy should also guarantee a certain level of accuracy. The key advantage of the frequency sampling method proposed in this paper is that it can select a new frequency sample by computing the difference between two responses obtained by two adjacent local ROMs. Such an adaptive procedure also provides the error of the constructed ROM, which is considered for an efficient frequency response analysis.

This paper is organized as follows: In Section 2, a mathematical formulation of the dynamic condensation procedure is revisited and a new algorithm for adaptive frequency sampling is proposed. Section 3 presents numerical examples for validating the accuracy and efficiency of the proposed method. In Section 4, conclusions and suggestions for future research topics are provided.

2. Mathematical Formulation

2.1. Frequency Response Analysis Based on Dynamic Condensation

We investigate a steady-state, time-harmonic response of a structural system. Let ω be an angular frequency and $\mathcal{S}$ be a bounded set in a frequency domain such that

$$\mathcal{S} = \left\{ \omega \in \mathbb{R}^+ \middle| \omega_L \leq \omega \leq \omega_U \right\}, \tag{1}$$

where $\mathbb{R}^+ := [0, \infty)$, and subscripts L and U are the lower and upper bounds of the frequency range of interest, respectively. Following previous expressions [33,35], the frequency response function of a spatially discretized matrix form of a finite element formulation can be written as follows:

$$\left(\mathbf{K} - \omega^2 \mathbf{M} + i\omega \mathbf{C} \right) \mathbf{u}(\omega) = \mathbf{Z}(\omega)\mathbf{u}(\omega) = \mathbf{f}(\omega), \tag{2}$$

where $\mathbf{M} \in \mathbb{R}^{N \times N}$, $\mathbf{C} \in \mathbb{R}^{N \times N}$, and $\mathbf{K} \in \mathbb{R}^{N \times N}$ are the mass, damping, and stiffness matrices, respectively, N represents the total degree of freedom of the system, and i is the imaginary number. The displacement vector and structural force input vector are $\mathbf{u} : \mathcal{S} \to \mathbb{C}^N$ and $\mathbf{f} : \mathcal{S} \to \mathbb{R}^N$, respectively. $\mathbf{Z}(\omega)$ represents an impedance matrix. Solving Equation (2) gives the frequency response of the system.

In the present study, we neglected the damping of the system without losing the generality of the proposed method. Previous research [38,39] has shown that even though we consider damping of the system resulting in a complex ROB matrix, the basic procedure of constructing ROM does not change, which is projecting high-dimensional field variables into low-dimensional space. Hence, the response vector is obtained as follows:

$$\mathbf{u}(\omega) = \mathbf{Z}(\omega)^{-1}\mathbf{f}(\omega) = \left(\mathbf{K} - \omega^2 \mathbf{M} \right)^{-1} \mathbf{f}(\omega). \tag{3}$$

In Equation (3), the response vector is the function of a frequency. In the rest of the paper, the dependency of $\mathbf{u}$ with respect to the frequency will be omitted since $\mathbf{u}$ is an output depending on the change of frequency.

As presented in the literature [11,13,14], deriving DOF-based ROM starts by dividing the degrees of freedom of a given system into master and slave ones such that

$$\begin{bmatrix} \mathbf{Z}_{mm}(\omega) & \mathbf{Z}_{ms}(\omega) \\ \mathbf{Z}_{sm}(\omega) & \mathbf{Z}_{ss}(\omega) \end{bmatrix} \begin{bmatrix} \mathbf{u}_m \\ \mathbf{u}_s \end{bmatrix} = \begin{bmatrix} \mathbf{f}_m(\omega) \\ \mathbf{f}_s(\omega) \end{bmatrix}, \tag{4}$$

where subscripts m and s denote master and slave DOFs, respectively. Using the notation of the subscript, $(\blacksquare)_{sm} = (\blacksquare)_{ms}^T$. Displacement vectors are $\mathbf{u}_s \in \mathbb{R}^{N_s}$ and $\mathbf{u}_m \in \mathbb{R}^{N_m}$, where N_s and N_m represent numbers of DOFs of slave and master ones, respectively. In general, $N_s \gg N_m$. Considering that DOF-based ROM can synchronize responses of the master DOF with sensor responses in actual structures, N_m is usually determined by the number

of sensors, which finally determines the size of the ROM. The relationship between master and slave DOF is derived from the lower part of Equation (4) as follows:

$$\mathbf{Z}_{sm}(\omega)\mathbf{u}_m + \mathbf{Z}_{ss}(\omega)\mathbf{u}_s = \mathbf{f}_s(\omega). \tag{5}$$

Consequently, displacement of the slave DOF can be expressed by the linear combination of the transformation matrix and the master DOF with a forcing term to the slave DOF as follows:

$$\mathbf{u}_s = \mathbf{t}(\omega)\mathbf{u}_m + \mathbf{Z}_{ss}^{-1}(\omega)\mathbf{f}_s(\omega), \tag{6}$$

where $\mathbf{t} : \mathcal{S} \to \mathbb{R}^{N_s \times N_m}$ is defined as

$$\mathbf{t}(\omega) := -\mathbf{Z}_{ss}^{-1}(\omega)\mathbf{Z}_{sm}(\omega). \tag{7}$$

Substituting Equation (6) into the upper part of Equation (4) results in a ROM with an unknown vector displacement of master DOF such that

$$\mathbf{Z}_R(\omega)\mathbf{u}_m = \mathbf{f}_R(\omega), \tag{8}$$

where

$$\mathbf{Z}_R(\omega) = \mathbf{Z}_{mm}(\omega) - \mathbf{Z}_{ms}(\omega)\mathbf{t}(\omega), \tag{9}$$

$$\mathbf{f}_R(\omega) = \mathbf{f}_m(\omega) - \mathbf{t}(\omega)^T\mathbf{f}_s(\omega). \tag{10}$$

For numerical frequency sweeping simulation, discrete frequency instances are selected in $\mathcal{S}$. Let the kth frequency instance be ω_k, a set of discrete frequencies is defined as follows:

$$\mathcal{S} = \{\omega_k | \omega_L \leq \omega_k \leq \omega_U\} \subset \mathcal{S}. \tag{11}$$

where $k = 1, 2, \ldots, N_\omega$. Thus, dynamic condensation is derived from the transformation matrix defined by $\mathbf{t}_k := \mathbf{t}(\omega_k)$. Successively the dynamic ROM by the Galerkin projection of Equation (3) using Equation (7) is obtained as follows:

$$\mathbf{u}_m(\omega_k) = \left(\mathbf{K}_{R,k} - \omega_k^2\mathbf{M}_{R,k}\right)^{-1}\mathbf{f}_{R,k}, \tag{12}$$

where

$$\mathbf{K}_{R,k} = \mathbf{K}_{mm} + \mathbf{t}_k^T\mathbf{K}_{sm} + \mathbf{K}_{ms}\mathbf{t}_k + \mathbf{t}_k^T\mathbf{K}_{ss}\mathbf{t}_k, \tag{13}$$

$$\mathbf{M}_{R,k} = \mathbf{M}_{mm} + \mathbf{t}_k^T\mathbf{M}_{sm} + \mathbf{M}_{ms}\mathbf{t}_k + \mathbf{t}_k^T\mathbf{M}_{ss}\mathbf{t}_k, \tag{14}$$

$$\mathbf{f}_{R,k} = \mathbf{f}_m + \mathbf{t}_k^T\mathbf{f}_s. \tag{15}$$

In Equation (12), system matrices and frequency are expressed explicitly without using the impedance matrix. From a computational point of view, the transformation matrix is computed at ω_k. Using Equations (13) and (14), reduced matrices are obtained. Successively, the final frequency response is obtained using Equation (12).

2.2. Multiple Local ROMs at Sample Frequencies

For the conventional dynamic reduction method, transformation $\mathbf{t}_k$ and reduced matrices $\mathbf{K}_{R,k}$ and $\mathbf{M}_{R,k}$ are constructed whenever the frequency changes, which increases computational cost due to the inversion of the impedance matrix with a size of $N_s \times N_s$. In this work. the framework of surrogate modeling is introduced, which builds multiple model surrogates in the offline stage and computes a response with a new input frequency in the online stage. In other words, dynamic ROMs are localized by solving high-fidelity

models at several frequency instances in the offline phase, and near, real-time responses are obtained by solving local ROMs in the online stage.

A set of frequency samples are first defined in a bounded range as follows:

$$\boldsymbol{S}_{(j)} = \left\{ \omega_{(j),k} \middle| \omega_{(j),L} \leq \omega_{(j),k} \leq \omega_{(j),U} \right\} \subset \boldsymbol{S}. \tag{16}$$

The subscript (j) denotes the jth range in $\boldsymbol{S}$ with $j = 1, 2, \ldots, N_R$. The union of each set becomes $\boldsymbol{S} = \boldsymbol{S}_{(1)} \cup \boldsymbol{S}_{(2)} \cup \cdots \cup \boldsymbol{S}_{(N_R)}$. Therefore, $\omega_L = \omega_{(1),L}$ and $\omega_U = \omega_{(N_R),U}$. The jth local ROM covers the frequency range in $\boldsymbol{S}_{(j)}$. It will be constructed in the middle point in $\boldsymbol{S}_{(j)}$, which is

$$\overline{\omega}_{(j)} = \frac{\omega_{(j),L} + \omega_{(j),U}}{2}, \tag{17}$$

where upper and lower bounds of the jth range are determined by the algorithm including an error estimation, which will be presented in the following section.

The middle point $\overline{\omega}_{(j)}$ becomes the jth sample frequency. Thus, the local ROM is constructed. Its response is computed as follows:

$$\mathbf{u}_m\left(\omega_{(j),k}\right) = \left(\mathbf{K}_{R(j)} - \omega_{(j),k}^2 \mathbf{M}_{R(j)}\right)^{-1} \mathbf{f}_{R(j)}. \tag{18}$$

where the system matrices are expressed using the notation without the upper bar, $\mathbf{t}_{(j)} := \mathbf{t}\left(\overline{\omega}_{(j)}\right)$ since system matrices are always evaluated at the sampling frequency. Additionally, note that the response vector $\mathbf{u}_m\left(\omega_{(j),k}\right)$ is an approximation except for $\omega_{(j),k} = \overline{\omega}_{(j)}$, as the ROM is constructed using a local ROB, $\mathbf{t}_{(j)}$.

Remark 1. *For the 1st and the N_Rth ranges, upper and lower bounds become sample frequencies. For example, $\overline{\omega}_{(1)} = \omega_L$ and $\overline{\omega}_{(N_R)} = \omega_U$. Thus, local ROMs at lower and upper bounds cover only the upper and lower half of each local range, respectively.*

Remark 2. *In the offline stage, $\boldsymbol{K}_{R(j)}$, $\boldsymbol{M}_{R(j)}$, and $\boldsymbol{f}_{R(j)}$ are constructed and saved. As a single reduced matrix contains only N_m^2 elements and the number of samples is adaptively determined by satisfying $N_R \ll N_\omega$, the proposed method does not require much memory for saving ROMs, which is also beneficial for efficient computation in the online stage.*

2.3. A New Adaptive Sampling Method and Construction of Local ROMs

Once displacement vectors are computed from local ROMs, the final response is obtained simply by stacking each vector in $\boldsymbol{S}$. However, as the local frequency range is set as defined in Equation (8), upper and lower bounds of adjacent range overlap with each, for example, $\omega_{(j),U} = \omega_{(j+1),L}$. There exists a gap between displacement vectors obtained at these bounds. In other words, approximated displacements from two adjacent ROMs at a single frequency are not the same since the approximation accuracy decreases if the difference between input and sampling frequencies increases. Let $\mathbf{u}_{m(j),k} := \mathbf{u}_m\left(\omega_{(j),k}\right)$, then the difference can be written as follows:

$$\Delta \mathbf{u}_m = \mathbf{u}_{m(j),U} - \mathbf{u}_{m(j+1),L}. \tag{19}$$

Thus, if the difference is greater than a specific criterion, another dynamic ROM is constructed at the point and the range that local ROM needs to be covered becomes narrow. This is a key idea of the new adaptive sampling method proposed in this paper.

In the proposed method, the first set of sample frequencies is determined by the user. The next sample set then becomes the union of the first set and additional samples. Let the

pth set of sample frequencies be $\mathbf{S}^{(p)}$, then elements within the domain of interest can be expressed as follows:

$$\mathbf{S}^{(p)} = \left\{ \overline{\omega}_{(1)}^{(p)}, \overline{\omega}_{(2)}^{(p)}, \cdots, \overline{\omega}_{(N_b^{(p)})}^{(p)} \right\}, \tag{20}$$

where the superscript (p) is used to designate the level of sampling, and $N_b^{(p)}$ denotes the number of frequency samples in the pth level. Although every mid-point of two adjacent samples should be evaluated for $p = 1$, only selected ranges where new samples have been added in the previous level are divided if $p \geq 2$. Let $\overline{\omega}_{c,q}^{(p)}$ be the qth candidate frequency to be evaluated in the jth range, which is expressed as follows:

$$\overline{\omega}_{c,q}^{(p)} = \frac{\overline{\omega}_{(j)}^{(p)} + \overline{\omega}_{(j+1)}^{(p)}}{2}. \tag{21}$$

As illustrated in Figure 1, there is no relationship between the candidate number q and the range number, j. Thus, a mapping of indices is required to designate the position of the candidate and adjacent samples, for example, $j = f^{(p)}(q)$, where $f^{(p)} : \mathrm{N} \to \mathrm{N}$. Once candidate frequencies on the pth level are determined, displacement vectors associated with candidates can be calculated using two adjacent local ROMs such that

$$\mathbf{u}_{m(j),U} = \left(\mathbf{K}_{R(j)} - \overline{\omega}_{c,q}^{(p)} \mathbf{M}_{R(j)} \right)^{-1} \mathbf{f}_{R(j)}, \tag{22}$$

$$\mathbf{u}_{m(j+1),L} = \left(\mathbf{K}_{R(j+1)} - \overline{\omega}_{c,q}^{(p)} \mathbf{M}_{R(j+1)} \right)^{-1} \mathbf{f}_{R(j+1)}, \tag{23}$$

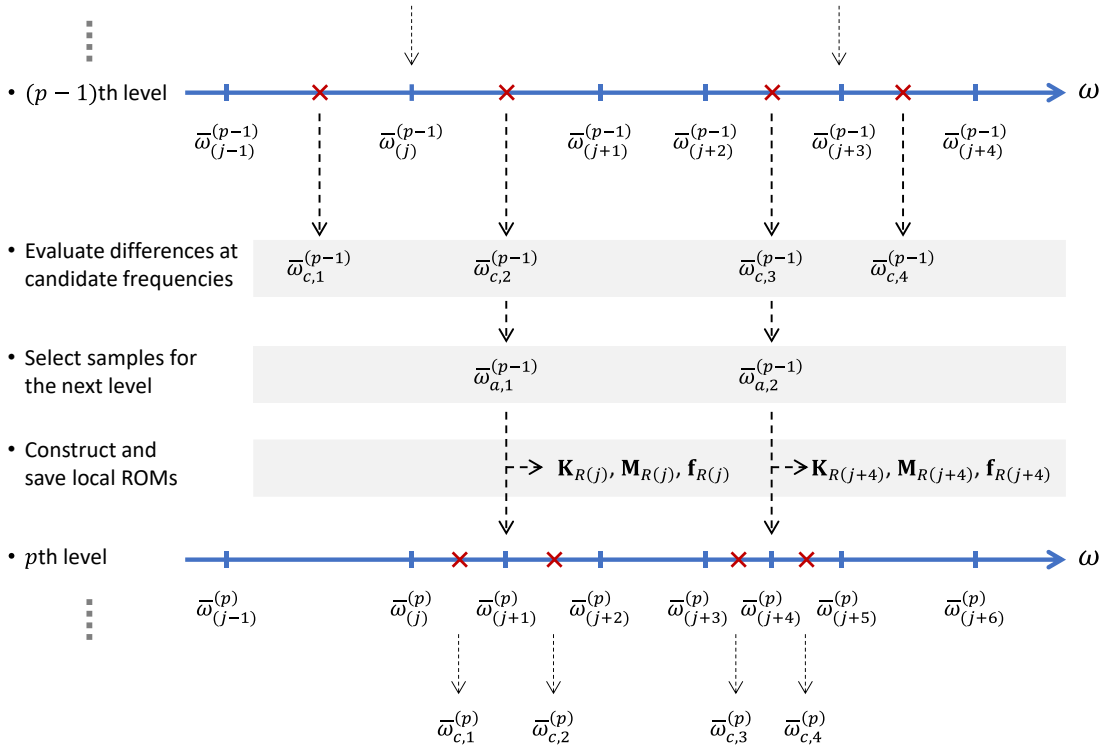

Figure 1. Schematic of the adaptive sampling algorithm with the construction of local ROMs in the frequency domain.

If the $\Delta\mathbf{u}_m$ in Equation (19) satisfies the criteria, for example, $|\Delta\mathbf{u}_m| < tol.$, $\overline{\omega}_{c,q}^{(p)}$ is not chosen as a new sample. Otherwise, the associated local ROM at $\overline{\omega}_{c,q}^{(p)}$ is constructed as

a new sample at the $(p+1)$th level. The overall process of selecting sample frequency and constructing local ROMs is presented in Algorithm 1, where the number of candidate frequencies and selected frequencies to be added to the next level are denoted by $N_c^{(p)}$ and $N_a^{(p)}$, respectively, and the set associated with selected frequencies is represented by $\boldsymbol{S}_a^{(p)}$. Thus, the number of elements is defined by the cardinality as $N_a^{(p)} := \mathbf{n}\left(\boldsymbol{S}_a^{(p)}\right)$. In fact, the numbers of candidates and selections have the following relationships except for $p = 1$ such that

$$N_b^{(p+1)} = N_b^{(p)} + N_a^{(p)}, \;\; N_c^{(p+1)} = 2N_a^{(p)}. \tag{24}$$

Algorithm 1 Adaptive Frequency Sampling and Local ROM Construction.

Define a set of frequency samples, $\boldsymbol{S}^{(1)}$ as in Equation (20)
$N_b^{(1)} \leftarrow \mathbf{n}\left(\boldsymbol{S}^{(1)}\right)$
$N_c^{(1)} \leftarrow N_b^{(1)} - 1$
for $j = 1, 2, \cdots, N_b^{(1)}$, **do**
  Compute $\mathbf{t}\left(\overline{\omega}_{(j)}^{(1)}\right)$ and $\mathbf{K}_{R(j)}$, $\mathbf{M}_{R(j)}$, $\mathbf{f}_{R(j)}$
  Compute $\mathbf{u}_{m(j)}$ as in Equation (18)
end for
Compute candidate frequencies, $\overline{\omega}_{c,q}^{(1)} \leftarrow \frac{\overline{\omega}_{(j)}^{(1)} + \overline{\omega}_{(j+1)}^{(1)}}{2}$, where $j = 1, 2, \cdots, N_c^{(1)}$
Construct a mapping from the index j to p as, $j \leftarrow f^{(1)}(q)$
$p \leftarrow 1$
while (1), **do**
  $\boldsymbol{S}_a^{(p)} \leftarrow \varnothing$, $r \leftarrow 0$
  for $q = 1, 2, \cdots, N_c^{(p)}$, **do**
    Compute $\mathbf{u}_{m(j),U}$ and $\mathbf{u}_{m(j+1),L}$ at $\overline{\omega}_{c,q}^{(p)}$ as in (22) and (23) with $j = f^{(p)}(q)$
    if $|\Delta \mathbf{u}_m| > tol$.
      $\overline{\omega}_{a,r}^{(p)} \leftarrow \overline{\omega}_{c,q}^{(p)}$, and map the indices, $q \leftarrow g^{(p)}(r)$
      $\boldsymbol{S}_a^{(p)} \leftarrow \boldsymbol{S}_a^{(p)} \cup \left\{\overline{\omega}_{a,r}^{(p)}\right\}$
      $r \leftarrow r + 1$
    end if
  end for
  if $r = 0$
    break
  else
    $N_a^{(p)} \leftarrow r$
    for $l = 1, 2, \cdots, N_a^{(p)}$, **do**
      Compute $\mathbf{t}\left(\overline{\omega}_{a,l}^{(p)}\right)$ and $\mathbf{K}_{R(N_b^{(p)}+l)}$, $\mathbf{M}_{R(N_b^{(p)}+l)}$, $\mathbf{f}_{R(N_b^{(p)}+l)}$
      Compute $\mathbf{u}_{m(N_b^{(p)}+l)}$ as in Equation (18).
      $\overline{\omega}_{c,q}^{(p+1)} \leftarrow \frac{\overline{\omega}_{(j)}^{(p)} + \overline{\omega}_{a,l}^{(p)}}{2}$ and $\overline{\omega}_{c,(q+1)}^{(p+1)} \leftarrow \frac{\overline{\omega}_{a,l}^{(p)} + \overline{\omega}_{(j+1)}^{(p)}}{2}$ with $j = f^{(p)}\left(g^{(p)}(l)\right)$
    end for
    Construct a mapping from the index j to q as, $j \leftarrow f^{(p+1)}(q)$
    $N_b^{(p+1)} \leftarrow N_b^{(p)} + N_a^{(p)}$
    $N_c^{(p+1)} \leftarrow 2N_a^{(p)}$
    $\boldsymbol{S}^{(p+1)} \leftarrow \boldsymbol{S}^{(p)} \cup \boldsymbol{S}_a^{(p)}$
    $p \leftarrow p + 1$
  end if
end while

Remark 3. *If we use uniform samples initially, which is not necessarily for the proposed method, the pth level candidate covers* $(1/2)^p(\omega_U - \omega_L)$ *ranges.*

Remark 4. *The relationship between tolerance and efficiency was not explicitly revealed in this study. As accuracy is also affected by the selection of the master DOF, tolerance-efficiency tradeoffs need to be further determined in the future.*

2.4. Frequency Response Analysis in the Online Phase

In the online phase, local ROMs are recalled depending on the frequency input. Assume that local ROMs satisfy the tolerance at all-sample frequencies on the pth level, then sets of frequency ranges can be expressed as follows:

$$\boldsymbol{S}_{(j)}^{(p)} = \left\{ \omega_{(j),k}^{(p)} \middle| \omega_{(j),L}^{(p)} \leq \omega_{(j),k}^{(p)} \leq \omega_{(j),U}^{(p)} \right\}. \tag{25}$$

where $j = 1, 2, \cdots, N_b^{(p)} - 1$. Sample frequency also satisfies $\overline{\omega}_{a,q}^{(p)} \in \boldsymbol{S}_{(j)}^{(p)}$ with $q = f^{(p)-1}(j)$. Finally, frequency responses in $\boldsymbol{S}_{(j)}^{(p)}$ are obtained using Equation (18).

Once all local responses corresponding to master DOFs are obtained, responses at the boundaries of sets need to be handled. Considering that each range overlaps with others, two distinct displacement vectors are obtained despite their difference being lower than the tolerance. In fact, a vector from either the upper or lower range can be selected for efficiency. Otherwise, the two vectors are simply averaged, increasing the accuracy of displacement at boundaries as follows:

$$\mathbf{u}_m\left(\overline{\omega}_{a,q}^{(p)}\right) = \frac{\mathbf{u}_{m(j),U} + \mathbf{u}_{m(j+1),L}}{2}. \tag{26}$$

Since reduced vectors represent a physical displacement for the DOF-based ROM, direct superposition of two vectors is possible unlike, for example, variables in the generalized coordinate system.

3. Numerical Examples

For assessment and verification of the proposed method, a simple M-K system, an L-shape plate, and a large-scale wing-box structure were investigated as representative examples. All simulations were conducted with MATLAB R2022b in Windows 11 environment. A 12-core CPU running at 4.3 GHz was used for computation.

3.1. Example 1: 16-DOF Mass-Spring System

Figure 2 shows a simple mass-spring system. The number of DOFs was set to 16 with $k_1 = k_2 = \cdots = k_{16} = 300$ N/m, and $m_1 = m_2 = \cdots = m_{16} = 1$ kg. Four random DOFs were selected as master DOF, which were 3, 7, 14, and DOF 16 was both master and input DOF. As investigated in previous studies [38,40], the selection of master DOF is another important topic in dynamic condensation. Although the selection of the master DOF affects the dynamic behavior of the ROM, their causality is not fully revealed yet. ROMs of the proposed method were obtained after determining master DOFs, and various selection algorithms are applicable, which should be completed before ROM construction. Thus, this paper focuses on the adaptive algorithm and its accuracy and efficiency. The frequency range was 0 to 3 Hz, and the number of frequencies was 3000, which was $\Delta\omega_k = 0.001$ with $\omega_{k+1} = \omega_k + \Delta\omega_k$, where $k = 1, 2, \ldots, 3000$.

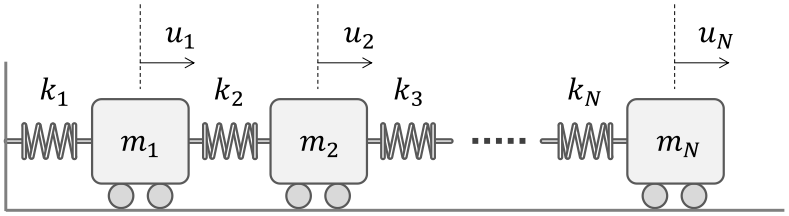

Figure 2. Example 1: A mass-spring system.

First, updates of sample positions are presented in Figure 3. For initial sampling, seven uniform instances were selected as shown in the first graph, with a 0.5 Hz gap between each sample. After running the algorithm, an update was conducted a total of eight times by setting the tolerance to 3% in the norm of the relative difference. New samples were adaptively selected at each level. An apparent increase in accuracy was observed for the proposed local ROM, particularly at earlier levels. For the eighth level, the frequency response of the ROM was almost the same as that of the FOM. At several positions around 1.25 Hz, 2.1 Hz, and 2.75 Hz, ranges were divided more than other regions, which proved that the coverage of the local ROM was not uniform due to the dependency of the dynamic transformation matrix on the frequency. In other words, local ROB guarantees the accuracy of the ROM in a limited range. As a result, the accuracy can change depending on the frequency of the instance. In fact, dynamic behaviors of a structure dramatically change at the eigenfrequency due to a change in the phase angle. However, the oscillating behavior does not change much between the two eigenfrequencies. Therefore, if the sampling frequency is near the eigenvalue, the coverage of the local ROB becomes narrow. Consequently, sample frequencies are distributed unevenly in the frequency domain. The proposed algorithm can resolve such properties by introducing an adaptive selection algorithm. In Figure 4, frequency responses and phase angles of the FOM, local ROM with initial samples, and the local FOM with final samples are plotted at each master DOF. The proposed method converged to the FOM even though the initial sample had a noticeable difference from the FOM.

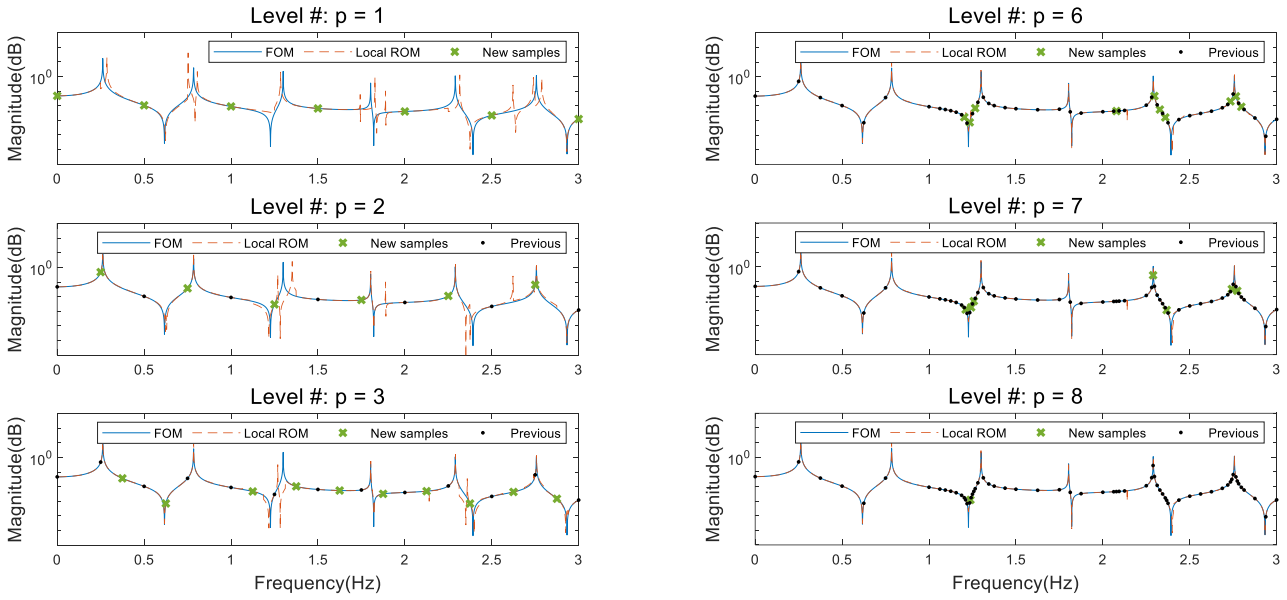

Figure 3. Adaptive selection of frequency instances and comparison of frequency responses of the FOM and local ROM (proposed) at DOF #14.

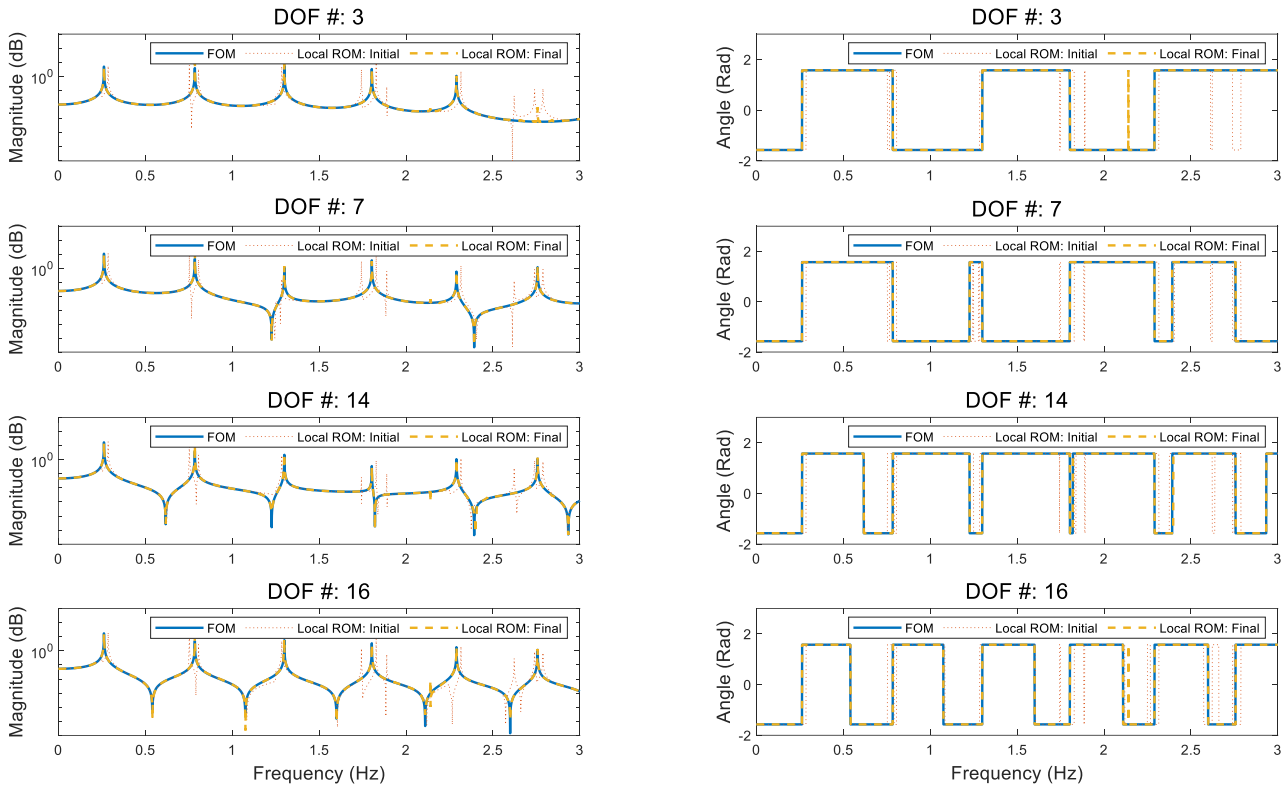

Figure 4. Comparison of frequency responses and phase angle at master DOF: (**a**) Frequency response; (**b**) Phase angle.

For quantitative comparisons, absolute and relative errors were evaluated. The absolute error was computed by the difference between the proposed method and the FOM at each frequency and the relative error was obtained as follows:

$$\boldsymbol{Err}(\omega_k) = \frac{1}{N_m}\sum_{j=1}^{N_m}\left|\frac{u^j_{FOM}(\omega_k) - u^j_{LROM}(\omega_k)}{u^j_{FOM}(\omega_k)}\right|, \tag{27}$$

where u^j is the jth component of a vector $\mathbf{u}$. Thus, at every $\omega_k \in \boldsymbol{S}$, the error was computed and averaged to the number of master DOF. As shown in Figure 5, each error was plotted, showing that both errors decreased depending on the level of the sample division. Particularly, near the mid-point of the initial sample showed the largest error. The error drastically decreased when $p = 3$. Figure 6 presents the average relative error depending on the sampling level. Furthermore, the tolerance of selecting a new sample point was changed from 10% to 1%. By decreasing the tolerance, both the accuracy and the level of the sampling increased. When $|\Delta\mathbf{u}_m| = 0.1$, the average relative error was 5.82%, and the number of samples was 39. For $|\Delta\mathbf{u}_m| = 0.01$, the error became 1.89%, and the sample number was 95. Considering the total number of frequency instances was 3000, 1.30% to 3.33% of frequencies resulted in errors of 1.89% to 5.82%.

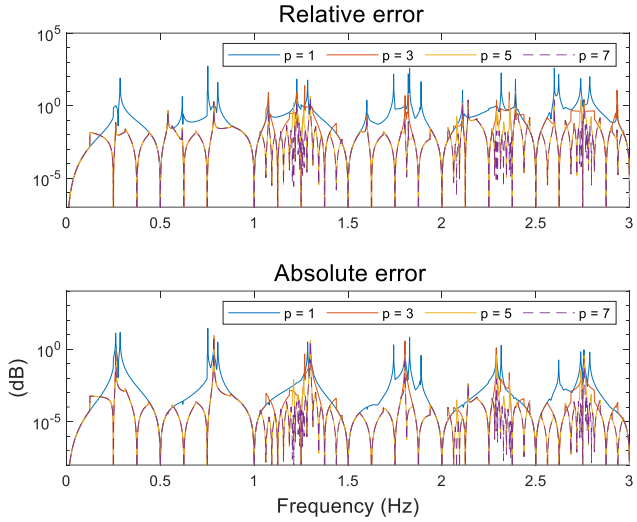

Figure 5. Relative and absolute errors of local ROMs (proposed) from FOM depending on the sampling level.

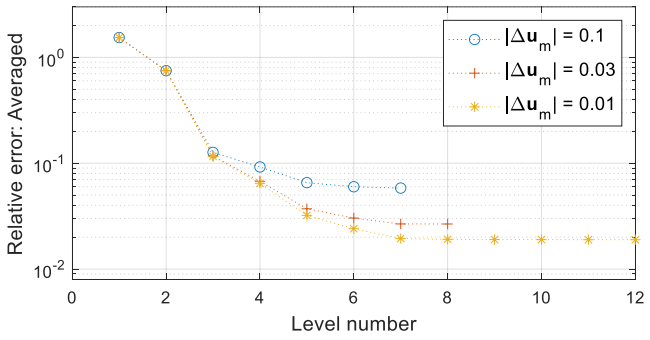

Figure 6. Averaged relative error depending on changing level of the sampling tolerance $|\Delta \mathbf{u}_m|$.

3.2. Example 2: L-Shaped Cantilever Plate

The second example used an L-shaped plate with one fixed end. Its geometry is shown in Figure 7, and the thickness was 0.1 m. Material properties were $E = 73.1$ GPa, $\nu = 0.33$, and $\rho = 2770$ kg/m^3. For finite element modeling, a discrete Kirchhoff triangular element was used. The numbers of elements and nodes were 294 and 176, respectively. Among 528 DOFs, six DOFs were selected as master ones, indicated by blue circles in Figure 7. The frequency input was applied to the corner of the plate indicated by a black arrow in Figure 7. The frequency range was 0–80 Hz, and 1600 instances were used with $\Delta\omega = 0.05$ Hz. For the first sampling, 11 frequencies including upper and lower bounds were selected with a uniform range.

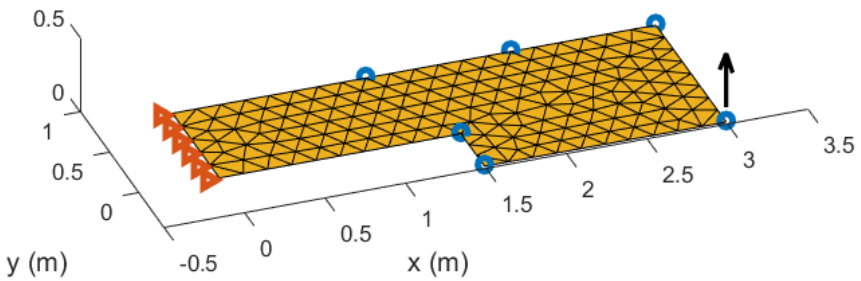

Figure 7. Example 2: An L-shaped cantilever plate.

In Figure 8, frequency responses of all master DOF are plotted to compare responses of the proposed method and those of the FOM with initial and final samples. The coordinates of each master DOF are presented in Table 1. Sampling tolerance was set to be within 3% of the relative difference. At every position of the master DOF, responses of local ROM well agreed with those of the FOM, although there were some deviations at the initial level.

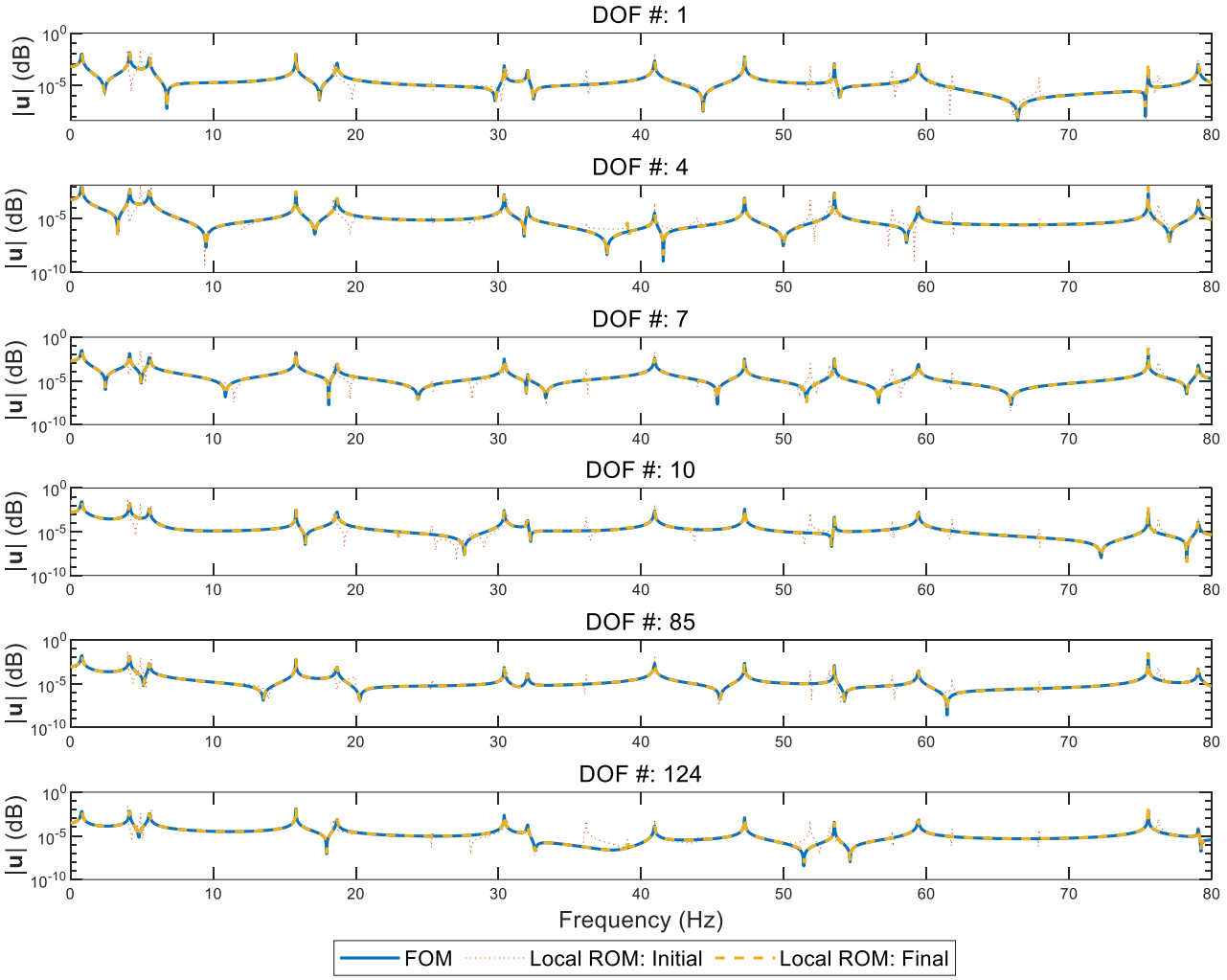

Figure 8. Comparison of frequency responses at master DOF.

Table 1. Coordinates and numbers of master DOF of example 2.

Master Node Number	x-coord. (m)	y-coord. (m)	Master DOF
1	1.5	−0.4	1
2	1.5	0	4
3	3	−0.4	7
4	3	0.8	10
29	2.1	0.8	85
42	1.2	0.8	124

Figure 9 shows decreases in relative errors averaged in the whole frequency range depending on the level number for four different tolerance cases. At the initial level, the relative error was over one as eleven samples among 1600 frequencies cannot appropriately describe the ROM's behavior. Accuracy jumps at the third level lowering the error to nearly 10% with 40 samples, which was almost four times the initial sample numbers.

As the tolerance decreased, the number of sampling levels and the accuracy of local ROM increased. When the tolerance was 10%, there was no further sampling after 6-time divisions of the selected range. The number of adaptive samples was 48, which was 3% of all frequency instances. The converged error was 5.97%. For 1% tolerance, 11-time updates were performed, resulting in 178 samples with an average relative error of 0.81%. Furthermore, the level of 3% tolerance was the same as that of 1%. The number of sample frequencies was 121, which was smaller than the 1% tolerance case. Although the accuracy of the proposed ROM was not exactly the same as the tolerance, the overall error of the ROM was close to the tolerance. Thus, the error level of local ROM might be roughly predicted. The exact prediction needs to be developed further, including the generalization of the proposed method to various dynamical systems. In Figure 10, the CPU time of each method was compared. The original dynamic ROM requires more computational resources than the FOM due to the projection of system matrices. For the proposed method, the online time was about 45.8 times faster than the FOM. Furthermore, the time for offline computation was much shorter than that of the FOM.

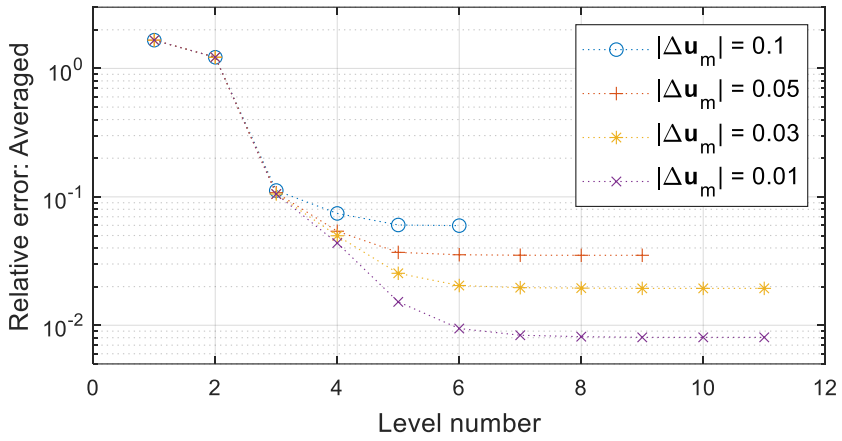

Figure 9. Averaged relative error depending on the changing level of sampling tolerance $|\Delta \mathbf{u}_m|$.

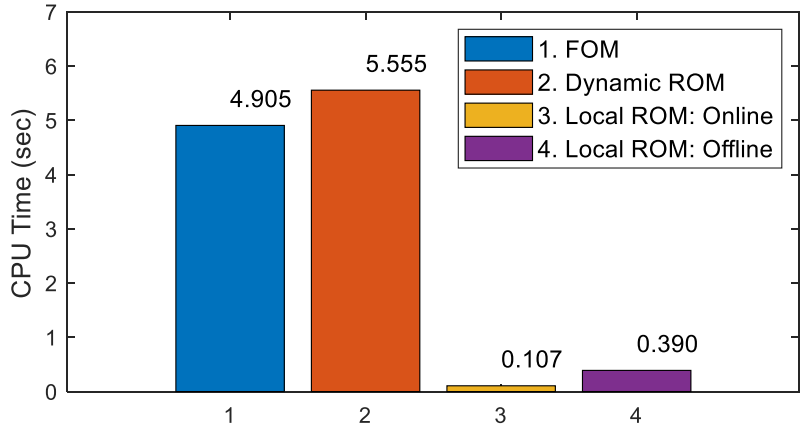

Figure 10. Comparison of computation time of FOM, dynamic ROM, and local ROMs.

3.3. Example 3: Wing-Box Model

The third example was a wing-box model consisting of upper and lower skins, five ribs, and five spars. The material was assumed to be aluminum with $E = 72$ GPa, $\nu = 0.3$, and $\rho = 2700$ kg/m^3. Semi-span of the wing was 14.94 m. The thicknesses of each part were $t_{U\_skin} = t_{L\_skin} = 3$ mm, $t_{ribs} = 5$ mm, and $t_{spars} = 7$ mm. They are represented using different colors in Figure 11. Regarding the finite element modeling, the MITC4 shell element was used. Thus, the wing structure had 12,560 elements and 12,073 nodes, and the total DOF was 72,438. The root of the wing was fixed, and the input was applied to the tip

of the wing, as denoted by a black arrow in Figure 11. A total of 11 DOFs were randomly selected as master DOF, including the loading position. Each node associated with the master DOF is presented as black circles in Figure 11. The frequency range was 3–10 Hz, and 7000 instances were used with $\Delta\omega = 0.001$ Hz. Initially, the sampling range was set to be 0.2 Hz, and the number of initial samples was 36, including upper and lower bounds.

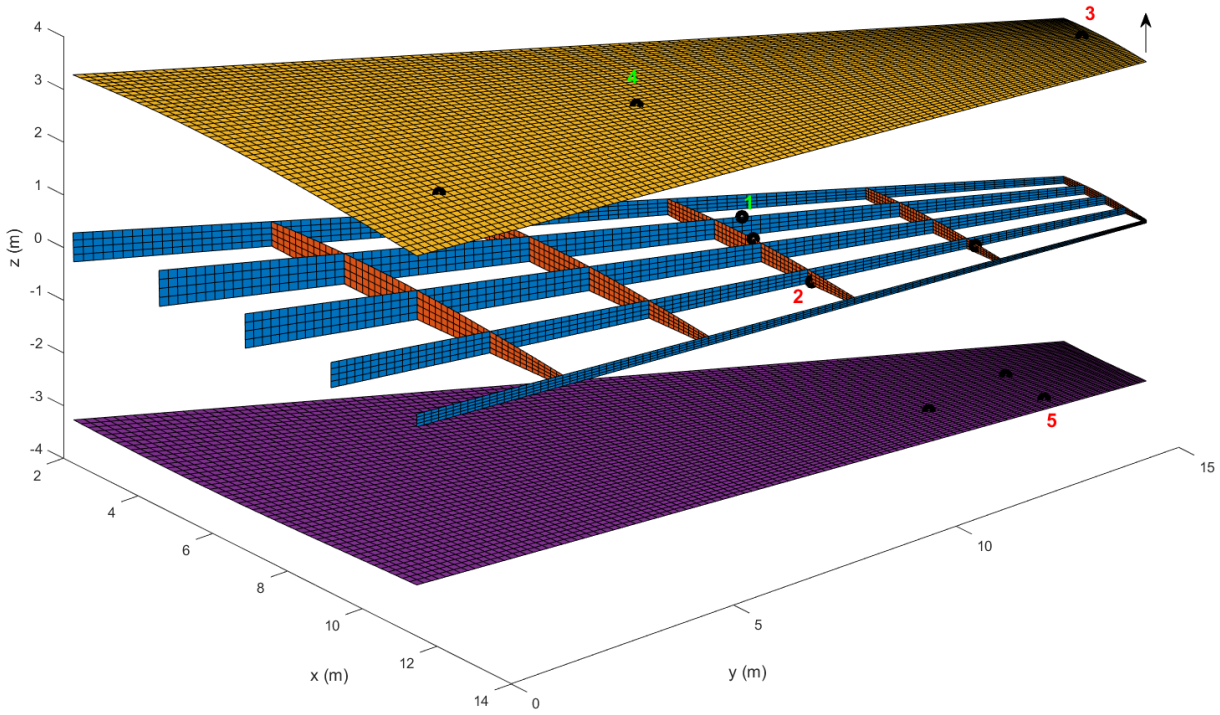

Figure 11. Example 3: A wing-box structure with a tip input, 11 master DOFs, and five selected DOFs.

In Figure 12, responses obtained by the proposed method with initial and final samples are plotted at each selected one among master DOFs. The frequency response showed more complex behavior than the previous two examples. Nevertheless, the proposed method approximated the result of the FOM including the 8–10 Hz region where there were a lot of frequency peaks. As the proposed sampling strategy adapts well to complex conditions from large-scale models, the proposed method is also expected to be universally applied to various structural analyses.

Figure 13 shows an averaged relative error of the proposed method depending on the tolerance of sampling. The tolerance changed from 10% to 5%, 3%, 1%, and 0.5%. As expected, the number of sampling levels and the accuracy of the ROM increased. Compared to previous examples, the gap between tolerance and average relative error was increased. As example 3 had larger frequency instances with more peak points than example 2, the overall error became larger than that of example 2. Figure 14 shows an efficiency comparison of the proposed method. The online time of the proposed method was 8349 times faster than the FOM. The offline time was also smaller than the FOM. In fact, the efficiency of the proposed method increases depending on the number of frequency instances. This proves the efficiency and usefulness of the proposed method, especially for large-scale dynamical systems.

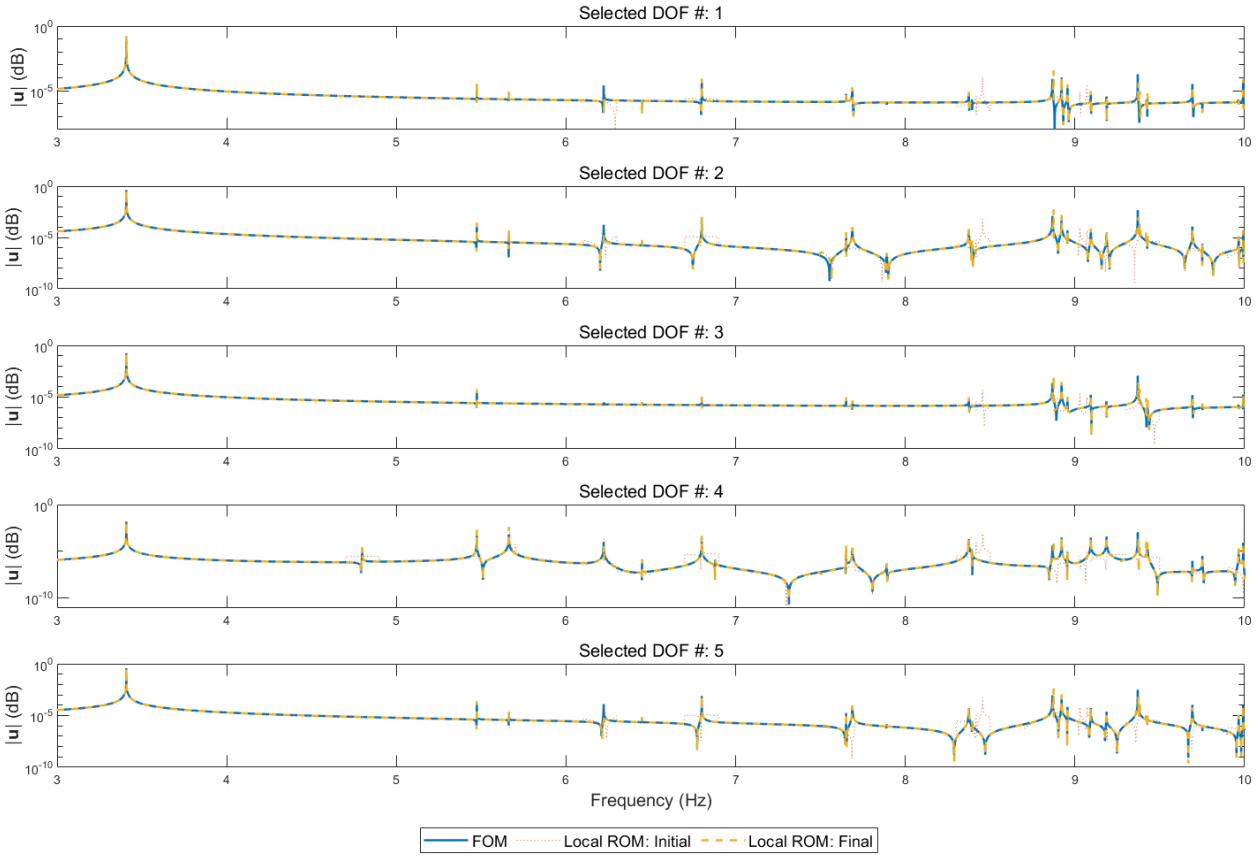

Figure 12. Comparison of frequency responses at selected master DOF.

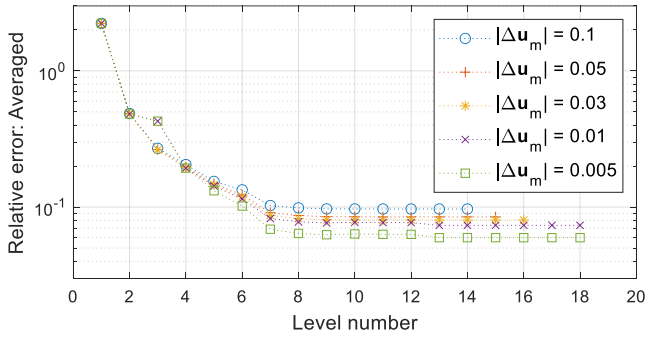

Figure 13. Averaged relative error depending on the changing level of the sampling tolerance $|\Delta \mathbf{u}_m|$.

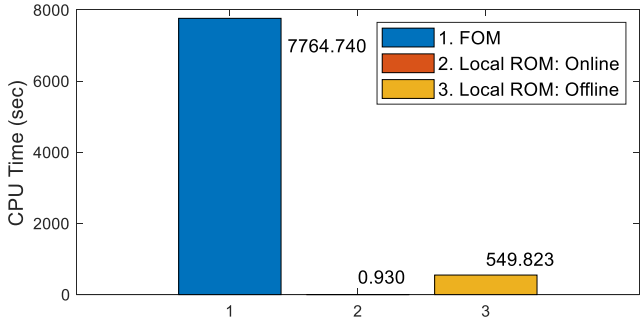

Figure 14. Comparison of computation time of FOM and local ROMs.

4. Conclusions

In this paper, a new frequency sampling algorithm was proposed within a framework of dynamic condensation-based reduced-order modeling. As the frequency response obtained by using DOF-based ROM does not need to be recovered, the efficiency in the online phase is guaranteed. Nevertheless, since the ROB becomes a function of frequency, implementing a global ROB that is applicable to the whole frequency range of interest is limited. Therefore, localizing the ROB and constructing multiple ROMs are suitable solutions for frequency response analysis of a large-scale structural system. Such a ROM construction process is regarded to be an offline stage where data are obtained by solving a full-scale, high-fidelity model in general. After that, responses are approximated using local ROMs in the online stage.

The proposed method was successfully applied to both offline and online stages. First, the evaluation of offline sampling was adaptively handled by estimating differences in responses computed at each sample point. In addition, an approximation of frequency response was efficiently performed in the online stage using local ROMs. Different from conventional ROMs that project the displacement vector into a generalized coordinate system, the reduced displacement vector of the proposed dynamic condensation-based method is in physical coordinates. Therefore, responses computed by local ROMs were directly stacked up, showing a possibility of real-time evaluation without additional treatments. Since the proposed method proved its efficiency and capability of adjusting accuracy within the offline-online framework, parametric variations such as initial, boundary, and loading conditions, material, and geometric properties of the system can be considered for future investigation. In fact, since the proposed method only considered frequency as an input parameter, the ROB needs to be changed in the form of a parametric reduced-order modeling method to take various parameters into account. Therefore, enhancing the proposed algorithm from a parametric modeling viewpoint is a desirable topic. Additionally, extending the proposed method to consider proportional and nonproportional damping effects is expected to develop efficient approximation in frequency sweeping of acoustic-structural combined analysis.

Author Contributions: Conceptualization, J.L. and S.C.; methodology, J.L. and S.C.; software, J.L., Y.P. and Y.L.; validation, J.L., Y.P. and Y.L.; formal analysis, J.L.; investigation, J.L. and S.C.; resources, J.L.; data curation, J.L., Y.P. and Y.L.; writing—original draft preparation, J.L.; writing—review and editing, J.L. and S.C.; visualization, Y.P. and Y.L.; supervision, J.L. and S.C. All authors have read and agreed to the published version of the manuscript.

Funding: This research was supported by the National Research Foundation of Korea, 2020 (NRF-2020R1C1C1011970), and by the National Research Foundation of Korea (NRF) grant funded by the Korean government (MSIT) (NRF-2018R1A5A7023490).

Data Availability Statement: Not applicable.

Conflicts of Interest: The authors declare no conflict of interest.

References

1. Lucia, D.J.; Beran, P.S.; Silva, W.A. Reduced-order modeling: New approaches for computational physics. *Prog. Aerosp. Sci.* **2004**, *40*, 51–117. [CrossRef]
2. Carlberg, K.T. Model Reduction of Nonlinear Mechanical Systems via Optimal Projection and Tensor Approximation. Ph.D. Thesis, Stanford University, Stanford, CA, USA, 2011.
3. Craig, R.R.; Kurdila, A.J. *Fundamentals of Structural Dynamics*, 2nd ed.; John Wiley & Sons: Hoboken, NJ, USA, 2006.
4. Kerschen, G.; Golinval, J.C.; Vakakis, A.F.; Bergman, L.A. The method of proper orthogonal decomposition for dynamical characterization and order reduction of mechanical systems: An overview. *Nonlinear Dyn.* **2005**, *41*, 147–169. [CrossRef]
5. Benner, P.; Gugercin, S.; Willcox, K. A survey of projection-based model reduction methods for parametric dynamical systems. *SIAM Rev.* **2015**, *57*, 483–531. [CrossRef]
6. Lee, J.; Lee, J.; Cho, H.; Kim, E.; Cho, M. Reduced-order modeling of nonlinear structural dynamical systems via element-wise stiffness evaluation procedure combined with hyper-reduction. *Comput. Mech.* **2021**, *67*, 523–540. [CrossRef]

7. Wan, Z.Y.; Vlachas, P.; Koumoutsakos, P.; Sapsis, T. Data-assisted reduced-order modeling of extreme events in complex dynamical systems. *PLoS ONE* **2018**, *13*, e0197704. [CrossRef] [PubMed]
8. Zhang, J.; Zheng, G. A mixed model reduction method for preserving selected physical information. *Mech. Syst. Signal Process.* **2017**, *86*, 224–236. [CrossRef]
9. Weng, S.; Tian, W.; Zhu, H.; Xia, Y.; Gao, F.; Zhang, Y.; Li, J. Dynamic condensation approach to calculation of structural responses and response sensitivities. *Mech. Syst. Signal Process.* **2017**, *88*, 302–317. [CrossRef]
10. Seilsepour, H.; Zarastvand, M.; Talebitooti, R. Acoustic insulation characteristics of sandwich composite shell systems with double curvature: The effect of nature of viscoelastic core. *J. Vib. Control* **2023**, *29*, 1076–1090. [CrossRef]
11. Koutsovasilis, P.; Beitelschmidt, M. Comparison of model reduction techniques for large mechanical systems: A study on an elastic rod. *Multibody Syst. Dyn.* **2008**, *20*, 111–128. [CrossRef]
12. Guyan, R.J. Reduction of stiffness and mass matrices. *AIAA J.* **1965**, *3*, 380. [CrossRef]
13. Friswell, M.I.; Garvey, S.D.; Penny, J.E.T. Model reduction using dynamic and iterated IRS techniques. *J. Sound Vib.* **1995**, *186*, 311–323. [CrossRef]
14. Xia, Y.; Lin, R.N. Improvement on the iterated IRS method for structural eigensolutions. *J. Sound Vib.* **2004**, *270*, 713–727. [CrossRef]
15. García-Illescas, M.A.; Alvarez-Icaza, L. Model reduction of shear building models: A quantitative approach for master degrees of freedom selection. *Eng. Struct.* **2019**, *179*, 512–522. [CrossRef]
16. Sung, H.; Chang, S.; Cho, M. Structural-system identification via a reduced system and the sensor-location selection method. *AIAA J.* **2019**, *57*, 2100–2108. [CrossRef]
17. Tian, W.; Weng, S.; Xia, Q.; Xia, Y. Dynamic condensation approach for response-based finite element model updating of large-scale structures. *J. Sound Vib.* **2021**, *506*, 116176. [CrossRef]
18. O'Callahan, J.C.; Avitabile, P.; Riemer, R. System equivalent reduction expansion process (SEREP). In Proceedings of the 7th International Modal Analysis Conference, Las Vegas, NV, USA, 30 January–2 February 1989.
19. Balmès, E. Parametric families of reduced finite element models. Theory and applications. *Mech. Syst. Signal Process.* **1996**, *10*, 381–394. [CrossRef]
20. Kim, T. Frequency-domain Karhunen-Loève method and its application to linear dynamic systems. *AIAA J.* **1998**, *36*, 2117–2123. [CrossRef]
21. Lee, J.; Cho, M. Efficient design optimization strategy for structural dynamic systems using a reduced basis method combined with an equivalent static load. *Struct. Multidiscip. Optim.* **2018**, *58*, 1489–1504. [CrossRef]
22. Amsallem, D.; Farhat, C. Interpolation method for adapting reduced-order models and application to aeroelasticity. *AIAA J.* **2008**, *46*, 1803–1813. [CrossRef]
23. Amsallem, D.; Cortial, J.; Carlberg, K.; Farhat, C. A method for interpolating on manifolds structural dynamics reduced-order models. *Int. J. Numer. Methods Eng.* **2009**, *80*, 1241–1258. [CrossRef]
24. Amsallem, D.; Farhat, C. An online method for interpolating linear parametric reduced-order models. *SIAM J. Sci. Comput.* **2011**, *33*, 2169–2198. [CrossRef]
25. Hong, S.K.; Epureanu, B.I.; Castanier, M.P.; Gorsich, D.J. Parametric reduced-order models for predicting the vibration response of complex structures with component damage and uncertainties. *J. Sound Vib.* **2011**, *330*, 1091–1110. [CrossRef]
26. Hong, S.K.; Epureanu, B.I.; Castanier, M.P. Next-generation parametric reduced-order models. *Mech. Syst. Signal Process.* **2013**, *37*, 403–421. [CrossRef]
27. Lee, J.; Cho, M. An interpolation-based parametric reduced order model combined with component mode synthesis. *Comput. Methods Appl. Mech. Eng.* **2017**, *319*, 258–286. [CrossRef]
28. Lee, J. A dynamic substructuring-based parametric reduced-order model considering the interpolation of free-interface substructural modes. *J. Mech. Sci. Tech.* **2018**, *32*, 5831–5838. [CrossRef]
29. Lee, J. A parametric reduced-order model using substructural mode selections and interpolation. *Comput. Struct.* **2019**, *212*, 199–214. [CrossRef]
30. Chang, S.; Cho, M. Dynamic-condensation-based reanalysis by using the Sherman–Morrison–Woodbury formula. *AIAA J.* **2021**, *59*, 905–911. [CrossRef]
31. Lee, J. An enhancement of the computational efficiency of parametric component mode synthesis within limited parameter domains using conventional interpolations. *Multiscale Sci. Eng.* **2022**, *4*, 66–72. [CrossRef]
32. Lee, J.; Kim, E.; Lee, J. Data reconstruction-based two-step non-intrusive reduced-order modeling using Fourier transform and interpolations. *Mathematics* **2022**, *10*, 3738. [CrossRef]
33. Avery, P.; Farhat, C.; Reese, G. Fast frequency sweep computations using a multi-point Padé-based reconstruction method and an efficient iterative solver. *Int. J. Numer. Methods Eng.* **2007**, *69*, 2848–2875. [CrossRef]
34. Tuck-Lee, J.P.; Pinsky, P.M. Adaptive frequency windowing for multifrequency solutions in structural acoustics based on the matrix Padé-via-Lanczos algorithm. *Int. J. Numer. Methods Eng.* **2008**, *73*, 728–746. [CrossRef]
35. Hetmaniuk, U.; Tezaur, R.; Farhat, C. Review and assessment of interpolatory model order reduction methods for frequency response structural dynamics and acoustics problems. *Int. J. Numer. Methods Eng.* **2012**, *90*, 1636–1662. [CrossRef]
36. Hetmaniuk, U.; Tezaur, R.; Farhat, C. An adaptive scheme for a class of interpolatory model reduction methods for frequency response problems. *Int. J. Numer. Methods Eng.* **2013**, *93*, 1109–1124. [CrossRef]

37. Binion, D.; Chen, X. A Krylov enhanced proper orthogonal decomposition method for frequency domain model reduction. *Eng. Comput.* **2017**, *34*, 285–306. [CrossRef]
38. Jeong, J.; Baek, S.; Cho, M. Dynamic condensation in a damped system through rational selection of primary degrees of freedom. *J. Sound Vib.* **2012**, *331*, 1655–1668. [CrossRef]
39. Esmaeilzad, A.; Khanlari, K. Dynamic condensation of non-classically damped structures using the method of Maclaurin expansion of the frequency response function in Laplace domain. *J. Sound Vib.* **2018**, *426*, 111–128. [CrossRef]
40. Kim, H.; Cho, M. Two-level scheme for selection of primary degrees of freedom and semi-analytic sensitivity based on the reduced system. *Comput. Methods Appl. Mech. Eng.* **2006**, *195*, 4244–4268. [CrossRef]